УДК 621.396.6

Microstrip Dual-Band Branch-Line Balun With Arbitrary Complex Frequency-Dependent Input and Load Impedances in Bands

Oborzhytskyy V. I., Fabirovskyy S. Ye., Storozh V. H., Matiieshyn Yu. M., Banshchykova T. Ye.

Lviv Polytechnic National University, Lviv, Ukraine

E-mail: *fabirovskii@gmail.com*

This article proposes a planar microstrip circuit configuration for designing a compact dual-band balun, whose two output signals have equal amplitudes and opposite phases in two operating frequency bands. At the same time, such circuit provides the transformation of complex load impedances different in these bands into the complex source input impedances, which also differ in these bands. The proposed balun circuit is based on a symmetric four-port branch line-based planar structure with one open port, formed by single-line segments with three reactive elements and an isolation scheme. To implement these reactive elements with different values across the frequency bands, transmission-line stubs are used. By applying even-odd mode analysis to the symmetrical four-port network, expressions were obtained for calculating the electrical parameters of the dual-band balun circuit elements. To remove restrictions on the transformable complex impedance values (both load and input), additional line segments are also introduced into this circuit, the parameters of which are set arbitrarily. The choice of the values of these parameters allows to provide as a result of calculations the electrical parameters of the line segments suitable for technical implementation. To verify the proposed circuit and calculation method, a prototype dual-band balun operating at 2.4 and 5.2 GHz was implemented and measured. To manufacture a balun based on microstrip transmission lines, a dielectric substrate with a dielectric constant of 2.6 and a thickness of 1.45 mm was used. Measurements showed that for amplitude and 180°-phase difference mismatches below 0.6 dB and 5°, respectively, the bandwidth of the dual-band balun is 290 MHz in both bands. Simulated and measured results agree well, proving the design concept.

Keywords: balun; dual-band operating; method of even-odd mode analysis; frequency-dependent input and termination impedances; complex impedance transforming

DOI: 10.64915/RADAP.2026.104.5-14

Introduction

A balun, as a three-port device used to convert a single-ended unbalanced signal into two differential balanced signals, plays a key role in modern wireless communication systems. In addition to forming signals at its outputs with equal magnitude but 180° out-of-phase, a balun can simultaneously perform other important functions. Such multifunctionality may include, for example, filtering properties, as implemented in [1–3]. The combination of a balun and a bandpass filter is achieved, for example in [1] by utilizing the inherent out-of-phase feature of the standing wave voltage distribution along an open-circuited half-wavelength microstrip transmission line loaded with multi-mode resonators from opposite sides. Another aspect of balun multifunctionality relates to the capability of transforming specific load impedance values at the outputs into a desired input impedance. Numerous publications discuss devices with such functions. The baluns proposed, for example, in [4–6] provide transformation of real impedances only, in [7–9] balun circuits for transforming complex impedances into real values have been developed, while the balun in [10] transforms complex impedances into a complex values. In addition to the aforementioned capabilities, options are offered with another balun function, namely, with work in two different frequency ranges. Such dual-band devices include those developed in [1, 2, 4–6, 8, 9]. When designing single-band baluns, the challenge of ensuring wide bandwidth is addressed. In such case, Defected Ground Structures (DGS) are often utilized, with a certain part of the circuit placed in the conductive layer (ground) [11,12], and double-layer or double-sided structures are also used [2, 13].

Generally, baluns, both with and without multifunctionality, differ in their circuit implementation. According to this approach, the following classification can be used: baluns based on a modification

of the Marchand scheme, for example [12–14], based on a modification of the Wilkinson divider [4, 15], based on the branch line configuration [5–7, 9, 10], based on a cascade connection of the coupled-line segments [8, 16, 17]. At the same time, most of the developed baluns, except for those based on modified dividers, feature, have a symmetrical four-port network structure where one port is either open- or short-circuited. For the resulting three-port circuit, it is possible to ensure core balun functions with input matching, output isolation, and output matching, while achieving multifunctionality. Analysis of existing balun circuits shows that the impedance transformation function is implemented almost exclusively in branch-line circuits and on the coupled-line segments. In most cases, only real values are transformed in both single-band [15,18] and dual-band [4–6,19] variants. Complex impedance transformation has been implemented only for single-band baluns [7,10,16]. Although dual-band baluns have been studied for many years, the dual-band conversion of complex load impedances to a real input impedance has been addressed in only two publications. Specifically, in [8] a variant based on four segments of coupled lines was proposed, and in [9] a balun with the same capabilities was implemented in the form of a branch-line structure. Notably, most known developments, with the exception of [12, 13, 15], have a planar implementation, which simplifies their manufacture using Printed Circuit Board (PCB) techniques.

In many cases of using baluns, such as in differential amplifier structures, balanced mixers, frequency multipliers, and antenna feed circuits, there is a need to transform complex load impedances into complex input impedance. A balun with this capability, especially in multiband systems, allows for a significantly reduce in system size due to the direct connection between the balun and the complex ports of external devices without additional matching circuits. However, no studies have been found that demonstrate dual-band transformation of complex impedances by a balun. One of the reasons for the lack of such developments is explained by the complexity of the problem of two-band transformation of complex impedances and the associated restrictions on permissible impedance values at which it is still possible to technically implement the transformer circuit elements according to its calculated electrical parameters. One of the solutions to such a problem we proposed in [20]. Therefore, the aim of this work is to develop a dual-band balun circuit capable of handling complex load and input impedances that differ across frequency bands, and the method for its calculation that avoids restrictions on the impedance values on both the input and load sides, as well as on the spacing of frequency bands. The circuit must be suitable for microstrip implementation using traditional PCB technology.

1 Choosing the Circuit of Balun and Its Analysis

Dual-band transformation of complex terminal impedances (i.e. the transformation of complex load impedances into complex input impedances), which should be provided by the balun, requires, according to [20], a stepped-impedance circuit consisting of five transmission line segments. A two-branch-line structure [9], which provides transformation of complex load impedances but only into real input impedance, was chosen as the basis for developing the dual-band balun with complex terminal impedances. Such a circuit is easy to fabricate using planar technology, and the solution to the problem of complex impedance transformation can be achieved by introducing additional single-line segments and reactive elements into the circuit. Fig. 1 shows the proposed circuit. Its electrical parameters (in the general form of writing) are the characteristic impedance Z_n and corresponding to them the electrical length θ_{ni}. The n index indicates that a parameter belongs to a specific segment: $n = 1S$ or $2S$ for the input-side segments, $n = 1L$ or $2L$ for the output-side segments, and $n = 1, 2,$ or 3 for the internal segments. The index i for the electrical length of the segments, as well as other circuit elements, which can take the value 1 or 2, indicates that the parameter corresponds to the center frequencies f_1 or f_2 of the first or second operating band, respectively. The circuit also includes reactive elements jX_{1i} and jX_{2i} with different values at the aforementioned frequencies, which is realized by a segment of the transmission line or a stepped connection of the segments.

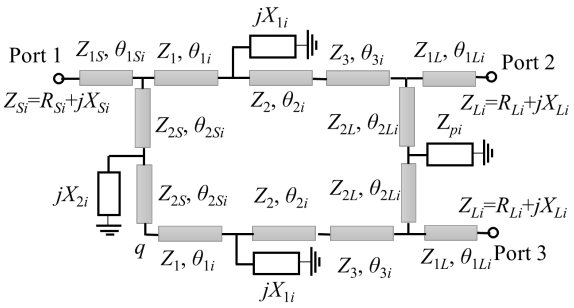

Fig. 1. Dual-band balun circuit

An important addition to the balun scheme from [9] is a single-line segment with parameters Z_{1S} and θ_{1Si} connected to the input port, where the circuit must provide a complex input impedance $Z_{Si} = R_{Si} + jX_{Si}$. Similar two single-line segments with parameters Z_{1L} and θ_{1Li} are placed on the output side, through which the load impedances $Z_{Li} = R_{Li} + jX_{Li}$ are connected to the circuit. Using these segments allows for overcoming restrictions on complex load impedances values Z_{Li} and complex input impedances Z_{Si}, different in frequency bands, and the restriction on the frequency ratio $k = f_2/f_1$, where f_2 is the central frequency of

the second higher operating band. The limitations arise because, at certain given values of these parameters, calculations of the characteristic impedances of one or more segments of line give values that do not fall within the technological limits permissible for stripline fabrication. The arbitrary choice of the values of the electrical parameters for the single-line segments with impedances Z_{1S} and Z_{1L}, as "free" circuit elements allows influencing the calculation process in order to ensure acceptable parameters of other segments. Such "free" elements also include branch line segments with parameters Z_{2S}, θ_{2Si} and Z_{2L}, θ_{2Li} which can be chosen arbitrarily. In Fig. 1, the equivalent complex impedance Z_{pi} represents the part of the balun circuit providing isolation and matching of its outputs.

The proposed balun circuit features to a four-port structure with longitudinal symmetry, where one port (point q in Fig. 1) is open-circuited with a reflection coefficient on it $\Gamma = 1$, converting the circuit into a three-port network. It is known [8], that to perform the function of a balun, the scattering parameters of such a three-port network must satisfy the following requirements: $S_{21} = -S_{31}$ (for equal of magnitude and antiphase output signals) and $S_{11} = S_{22} = S_{33} = S_{32} = 0$ (for matching and isolation). These conditions for symmetric four-port network are expressed via the scattering parameters of partial two-port networks under even- and odd-mode excitation. Thus, the condition for equal amplitude and anti-phase signals is written as $S_{21e} = 0$, while the condition for output ports matching and isolation is $S_{22e} = 0$. The subscript e indicates parameters belonging to the even-mode excitation partial networks. The input matching condition is defined as $Z_{even} + Z_{odd} = 2Z_s$, where Z_{even} and Z_{odd} are the input impedances of the even- and odd-mode partial networks, and Z_s is the source impedance. If $Z_{even} = 0$ ensured, the input matching condition simplifies to $Z_{odd} = 2Z_s$.

Thus, based on the above conditions, the balun design follows a two-stage process. At the first stage, the parameters of the elements of the odd-mode excitation circuit are determined, under which impedance transformation is ensured alongside the input matching. The second stage determines the parameters of the elements of the even-mode excitation circuit, at which the remaining of the functional conditions for the balun circuit are fulfilled.

Initial data for the calculation process includes operating frequencies f_1 and f_2, complex load impedances $Z_{L1} = R_{L1} + jX_{L1}$, $Z_{L2} = R_{L2} + jX_{L2}$, and complex input impedances $Z_{S1} = R_{S1} + jX_{S1}$, $Z_{S2} = R_{S2} + jX_{S2}$. Since the circuit utilizes parallel stubs and reactive elements, characteristic admittances $Y_n = 1/Z_n$ and the nodal admittances are used for analysis. In addition, at $i = 2$, i.e., at the frequency f_2, the electrical length of all segments of line is defined as $\theta_{n2} = k\theta_{n1}$, where θ_{n1} is the electrical length of segment at f_1 and k is a frequency ratio. In the analytical expressions below for the tangent function of electrical length, the following notation is used: $t_{ni} = \tan\theta_{ni}$, where the values of index n for line segments are the same as indicated above.

2 Impedance Transformation with Input Matching

The partial two-port circuit obtained from the general balun circuit under odd-mode excitation is shown in Fig. 2. To achieve the input matching with the simultaneous transformation of load impedances Z_{Li} into the input impedances Z_{Si}, this circuit must satisfy the equality $Z_{oddai} = 2Z_{a1i}$, where Z_{oddai} is the input impedance at node a in Fig. 2. The value of the impedance Z_{a1i} must be such that the line segment with Z_{1S} transforms it from node a into the given input impedance Z_{Si}. For this circuit, the parameters of the "free" elements $Z_{1S}, \theta_{1S1}, Z_{2S}, \theta_{2S1}$ and $Z_{1L}, \theta_{1L1}, Z_{2L}, \theta_{2L1}$ are set arbitrarily.

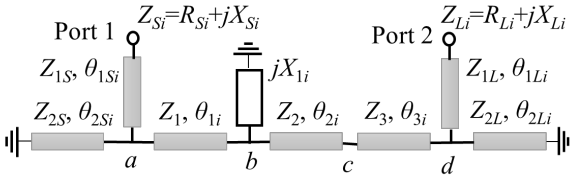

Fig. 2. Odd-mode equivalent circuit of the proposed dual-band balun

The transformation of complex impedances is performed following the sequence described in [20]. The total admittance Y_{di} at node d is given by:

$$Y_{di} = Y_{d1i} + Y_{d2i} = G_{di} + jB_{di}, \tag{1}$$

where $Y_{d1i} = Y_{1L}\frac{Y_{Li}+jY_{1L}t_{1Li}}{Y_{1L}+jY_{Li}t_{1Li}} = G_{d1i} + jB_{d1i}$, is the result of transformation of the load admittance $Y_{Li} = 1/Z_{Li}$ through the segment with Z_{1L}, θ_{1Li} into node d and $Y_{d2i} = -jY_{2L}/t_{2Li} = jB_{d2i}$ is the input admittance of the shorted stub with Z_{2L}, θ_{2Li}. The parameters Z_3, θ_{3i} of the segment that transforms Y_{di} into the admittance Y_{ci} at node c – with complex conjugate values at frequencies f_1 and f_2 (i.e., $Y_{c1} = G_c + jB_{c1}$ and $Y_{c2} = G_c - jB_{c1}$) – are determined by the following relations:

$$Y_3 = \sqrt{\begin{array}{l} G_{d1}G_{d2} + B_{d1}B_{d2} - \\ -\dfrac{(B_{d1}+B_{d2})(G_{d1}B_{d2} - G_{d2}B_{d1})}{G_{d1} - G_{d2}} \end{array}}, \tag{2}$$

$$\begin{aligned} \theta_{31} &= \frac{n_d\pi + \arctan\left(Y_3\frac{G_{d1}-G_{d2}}{G_{d1}B_{d2}-G_{d2}B_{d1}}\right)}{1+k}, \\ \theta_{32} &= k\theta_{31}, \end{aligned} \tag{3}$$

where n_d is chosen as an integer (0, 1, 2, ...). In this case, the real and imaginary parts of the admittance Y_{ci} are:

$$G_c = Y_3^2 \cdot \frac{G_{d1}(1+t_{31}^2)}{(Y_3 - B_{d1}t_{31})^2 + G_{d1}^2 t_{31}^2}, \tag{4}$$

$$B_{c1} = -B_{c2} = \\ = Y_3 \cdot \frac{Y_3 B_{d1}(1-t_{31}^2) + t_{31}(Y_3^2 - G_{d1}^2 - B_{d1}^2)}{(Y_3 - B_{d1}t_{31})^2 + G_{d1}^2 t_{31}^2}. \tag{5}$$

Next, we consider the transformation at the circuit input. The input admittance Y_{ai} of the right part of the circuit relative to node a is determined by:

$$Y_{ai} = \frac{1}{2}Y_{a1i} - Y_{a2i} = G_{ai} + jB_{ai}, \tag{6}$$

where $Y_{a1i} = Y_{1S} \cdot \frac{Y_{Si} - jY_{1S}t_{1Si}}{Y_{1S} - jY_{Si}t_{1Si}} = G_{a1i} + jB_{a1i}$ is the input admittance transformed by the segment with Z_{1S}, θ_{1Si} from node a into the signal admittance $Y_{Si} = 1/Z_{Si}$, and $Y_{a2i} = -jY_{2S}/t_{2Si} = jB_{a2i}$ is the input admittance of the shorted stub with Z_{2S}, θ_{2Si}. The use of half the value of Y_{a1i} in expression (6) is due to the matching condition, which requires the input impedance at node a to be $2Z_{a1i}$, and consequently, the admittance to be $Y_{a1i}/2$.

The line segment with parameters Z_1, θ_{1i} transforms the admittance Y_{bi} at node b – with complex conjugate values at frequencies f_1 and f_2, (i.e. $Y_{b1} = G_b + jB_{b1}$ and $Y_{b2} = G_b - jB_{b1}$) – to the value Y_{ai}. For this transformation, the impedance Z_1 must be calculated using formula (2) replacing G_{d1}, G_{d2} with G_{a1}, G_{a2} and B_{d1}, B_{d2} with B_{a1}, B_{a2}. The electrical length θ_{11} of this segment is defined as:

$$\theta_{11} = \frac{n_a\pi + \arctan\left(Y_1 \frac{G_{a1}-G_{a2}}{G_{a2}B_{a1} - G_{a1}B_{a2}}\right)}{1+k}, \\ \theta_{12} = k\theta_{11}, \tag{7}$$

where n_a is chosen as an integer (0, 1, 2, ...). In this case, the real and imaginary parts of Y_{bi} are:

$$G_b = Y_1^2 \left(\frac{G_{a1}(1+t_{11}^2)}{(Y_1 + B_{a1}t_{11})^2 + G_{a1}^2 t_{11}^2} \right), \tag{8}$$

$$B_{b1} = -B_{b2} = \\ = Y_1 \cdot \frac{Y_1 B_{a1}(1 - t_{11}^2) + t_{11}(G_{a1}^2 + B_{a1}^2 - Y_1^2)}{(Y_1 + B_{a1}t_{11})^2 + G_{a1}^2 t_{11}^2}. \tag{9}$$

The admittance Y_{ci} at node c is transformed by the segment with Z_2, θ_{2i} into the complex conjugate admittance Y_{bci} with a real part equal to G_b. For this purpose, $\theta_{2i} = m\pi/(k+1)$ is assumed, and Z_2 is determined from the equation:

$$Y_2^2 a + 2Y_2 b t_{21} + c t_{21}^2 = 0, \tag{10}$$

where m is typically 1 or 2; $a = G_c\left(1 + t_{21}^2\right) - G_b$, $b = G_b B_{c1}$, $c = -G_b\left(G_c^2 + B_{c1}^2\right)$. In this case, the imaginary part of the admittance Y_{bci} is:

$$B_{bc1} = -B_{bc2} = \\ = Y_2 \frac{Y_2 B_{c1}\left(1 - t_{21}^2\right) + t_{21}\left(Y_2^2 - G_c^2 - B_{c1}^2\right)}{(Y_2 - B_{c1}t_{21})^2 + G_c^2 t_{21}^2}. \tag{11}$$

The reactive element jX_{1i} ensures the equality $B_{bc1} + B_{11} = B_{b1}$, where $B_{11} = -1/X_{11}$. From this, we find:

$$B_{11} = B_{b1} - B_{bc1}, \\ B_{12} = -B_{11}. \tag{12}$$

This reactance, with opposite values at frequencies f_1 and f_2, is implemented by a stub with an electrical length of $\theta_{x1} = \pi/(k+1)$ and a characteristic impedance $Z_x = -1/t_{x1}B_{11}$ for a shorted end, or $Z_x = t_{x1}B_{11}$ for an open end, where $t_{x1} = \tan\theta_{x1}$. The input admittance Y_{bi} at node b is transformed to Y_{ai}, which ensures that the input matching condition at node a is met simultaneously with the dual-band transformation of the complex load impedance.

3 Output Ports Matching and Isolation

To ensure equal magnitudes and out-of-phase output signals, as well as outputs matching and isolation, the partial even-mode excitation circuit, as mentioned above, must be matched at the load side with a zero transmission coefficient. This circuit, derived from the general balun circuit, is shown in Fig. 3.

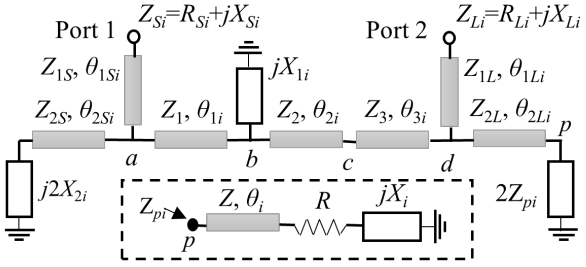

Fig. 3. Even-mode equivalent circuit of the proposed dual-band balun

The condition $S_{21e} = 0$ is achieved by short-circuiting node a, which provides zero input resistance of the stub loaded with double reactance jX_{2i}, which in this case is:

$$X_{2i} = -\frac{1}{2}Z_{2S}t_{2Si}. \tag{13}$$

In order to ensure the matching of Port 2 (to fulfill the condition $S_{22e} = 0$), it is necessary that the sum of the input admittance Y_{li} of the left relative to node d part of the circuit and the input admittance Y_{ri} of the

right part be a complex conjugate to the admittance $Y_{d1i} = G_{d1i} + jB_{d1i}$, determined by formula (1). For the input admittance Y_{li} of the left part, shorted at node a, which is the reactive conductance jB_{li}, and which is determined by successive transformation of the input admittance from node b to node c by a segment with Z_2 and then to node d by a segment with Z_3, it can be written:

$$B_{li} = Y_3 \cdot \frac{B_{cli} + Y_3 t_{3i}}{Y_3 - B_{cli} t_{3i}}, \tag{14}$$

where $B_{cli} = Y_2 \cdot \frac{B_{bli} + Y_2 t_{2i}}{Y_2 - B_{bli} t_{2i}}$, and $B_{bli} = -\left(\frac{1}{Z_1 t_{1i}} + \frac{1}{X_{1i}}\right)$. Hence, the input admittance Y_{ri} of the right part, formed by a stub with double load impedance Z_{pi}, is defined as the difference between the complex conjugate of the admittance Y_{d1i}, i.e., $G_{d1i} - jB_{d1i}$, and the admittance of the circuit left part:

$$Y_{ri} = G_{ri} + jB_{ri} = G_{d1i} - j\left(B_{d1i} + B_{li}\right). \tag{15}$$

Since this input admittance is the result of the transformation of the impedance $2Z_{pi}$ by a segment with Z_{2L}, then from the transformation expression, the ratios for calculating the real G_{pi} and imaginary B_{pi} components of the admittance $Y_{pi} = 1/Z_{pi}$ are written in form:

$$G_{pi} = 2\frac{G_{ri} Y_{2L}^2 \left(1 + t_{2Li}^2\right)}{G_{ri}^2 t_{2Li}^2 + \left(Y_{2L} + B_{ri} t_{2Li}\right)^2}, \tag{16}$$

$$B_{pi} = \frac{2G_{ri} Y_{2L} - G_{pi}\left(Y_{2L} + B_{ri} t_{2Li}\right)}{G_{ri} t_{2Li}}. \tag{17}$$

The part of the general balun circuit that provides isolation of its outputs and which is replaced in Fig. 1 by the equivalent impedance Z_{pi} must necessarily contain resistance, since the impedance $Z_{pi} = 1/(G_{pi} + jB_{pi}) = R_{pi} + jX_{pi}$ has the real part R_{pi} in its composition. Such a circuit, which in Fig. 3 is bounded by a dotted line, consists of a transmission line segment with parameters Z and θ_i, connected in series with a resistance R and a reactance jX_i. To calculate the parameters of these elements, an arbitrary value of the electrical length θ_1 is given and, based on the components of Z_{pi}, the characteristic impedance Z is determined from the equation:

$$Z^2 a_p + 2Z b_p + c_p = 0, \tag{18}$$

where $a_p = R_{p2}\left(1 + t_{p2}^2\right) - R_{p1}\left(1 + t_{p1}^2\right)$, $b_p = R_{p2} X_{p1} t_{p1}\left(1 + t_{p2}^2\right) - R_{p1} X_{p2} t_{p2}\left(1 + t_{p1}^2\right)$, $c_p = Z_{m1} R_{p2} t_{p1}^2\left(1 + t_{p2}^2\right) - Z_{m2} R_{p1} t_{p2}^2\left(1 + t_{p1}^2\right)$, $Z_{mi} = R_{pi}^2 + X_{pi}^2$, and $t_{pi} = \tan\theta_i$, $\theta_2 = k\theta_1$. The calculation of the resistance parameters R and reactance X_i is carried out using the following expressions:

$$R = \frac{Z^2 R_{p1}\left(1 + t_{p1}^2\right)}{Z^2 + 2ZX_{p1} t_{p1} + t_{p1}^2 Z_{m1}}, \tag{19}$$

$$X_i = \frac{Z\left(R_{pi} - R\right) - RX_{pi} t_{pi}}{R_{pi} t_{pi}}. \tag{20}$$

4 Sequence of Calculation of a Dual-Band Balun

The initial data for calculating a dual-band balun are the values of the parameters Z_{Si}, Z_{Li}, f_1 and f_2. The calculation is performed using the aforementioned expressions and formulas in the described sequence. First, the parameters of the line segments serving as "free" elements are set: the characteristic impedances Z_{1L}, Z_{2L} and the electrical lengths θ_{1L1}, θ_{2L1}. While the electrical parameters of these elements are chosen arbitrarily, they must remain within the physical limits required for the technical implementation of the segments. The electrical length can be selected in the range from 0 to 2π rad (from 0 to λ), and the permissible characteristic impedance limits – which primarily depend on the parameters of the dielectric substrate – must be determined beforehand using a characteristic impedance calculator. Subsequently, the admittance values Y_{di} are calculated using (1), and parameters Y_3, θ_{31} of the third line segment are determined via formula (2) and (3) with a selected integer value for n_d. If the solution to (2) yields Z_3 values that are unacceptable for physical implementation, the issue is addressed by adjusting the parameters of the previously set free elements. Using the parameters of the third segment, the components of the admittance Y_{ci} are calculated by (4) and (5).

Next, the parameters Z_{1S}, θ_{1S1}, Z_{2S}, θ_{2S1} for the input-side free elements are established. Admittance values Y_{ai} are calculated according to (6); based on these components, the parameters Y_1, θ_{11} of the first line segment are determined using formula (2) (with the appropriate substitution) and (7) for a chosen value of n_a. If (2) yields Z_1 values unsuitable for fabrication, one or more free element parameters must be adjusted. Using the first segment's parameters, the components of admittance Y_{bi} are calculated via (8) and (9).

Then, the parameter m is set to calculate the electrical length $\theta_{21} = m\pi/(k+1)$ for the second line segment. The characteristic admittance of this segment is then derived from (10). If (10) results in an unacceptable Z_2 value, the parameter m or other free element parameters must be modified. Subsequently, the susceptance values B_{bci} are calculated using (11), and the susceptance value B_{1i} is determined via (12), from which the reactance values X_{1i} are determined. This reactance is implemented using a stub.

This is followed by calculating the element parameters that ensure outputs matching and isolation. Reactance values X_{2i} for both frequencies are calculated per (13). Furthermore, the susceptance B_{li} and admittance Y_{ri} for the left and right portions of the even-mode excitation circuit are calculated using (14)

and (15). These values are then used to determine the real and imaginary components of the admittance Y_{pi} according to (16) and (17). After setting the electrical length θ_1 of the isolation circuit's single-line segment, its characteristic impedance Z is found from (18). If Z is physically unfeasible, θ_1 must be changed. Finally, the values for elements R and X_i of the isolation circuit are calculated using (19) and (20). The reactive elements X_{2i} and X_i, the values of which for two frequencies were obtained as a result of calculations, can be implemented, as indicated, for example, in [21], using a one- or two-stepped line stub.

5 Design Example of Dual-Band Balun

To verify the proposed design theory, a dual-band balun prototype was designed, fabricated and tested. The operating frequencies were selected as 2.4 and 5.2 GHz ($k = 2.17$). The complex impedances were chosen $(58.4-j5.35)/(56.8+j6.8)$ Ω for the input port and $(53.8+j13.4)/(69.9+j26.3)$ Ω for the output ports at 2.4/ 5.2 GHz, respectively. For the microstrip implementation, a dielectric substrate with a dielectric constant of 2.6, a loss tangent of 0.001 and a thickness of 1.45 mm was utilized. For the selected substrate, the permissible values of characteristic impedances of free and other line segments range from 40 Ω to 125 Ω, which for a microwave line corresponds to a central conductor width of 0.6–5.5 mm. To perform measurements using a network analyzer, the chosen complex input and output impedances were obtained by converting the 50 Ω impedance of the SMA connectors via transmission line segments. The dimensions of the line segment located between port 1 and the balun input, which transforms the complex balun input impedance to 50 Ω, are 3.4 mm width and 14.2 mm in length. This corresponds to a characteristic impedance of 55.59 Ω and an electrical length of 60.21° at 2.4 GHz. The line segments transforming the 50 Ω SMA connectors into complex load impedances of the balun are 2.2 mm wide and 5.2 mm long (characteristic impedance of 71.38 Ω and an electrical length of 21.71° at 2.4 GHz). These segments are located between the balun outputs and the ports 2 and 3. The initial values of the parameters for this prototype, calculated following the procedure described above, are (in the order of their definition): $Z_{1L} = 60$ Ω, $\theta_{1L1} = 40°$, $Z_{2L} = 60$ Ω, $\theta_{2L1} = 53°$, $Z_3 = 95.57$ Ω, $n_d = 1$, $\theta_{31} = 54.69°$, $Z_{2S} = 75$ Ω, $\theta_{2S1} = 56.84°$, $Z_1 = 68.94$ Ω, $n_a = 1$, $\theta_{11} = 56.54°$, $m = 1$, $\theta_{21} = 56.84°$, $Z_2 = 100.09$ Ω, $X_{11} = j85.37$ Ω, $X_{12} = -j85.37$ Ω, $X_{21} = -j57.40$ Ω, $X_{22} = j57.40$ Ω, $\theta_1 = 60.84°$, $Z = 55.01$ Ω, $R = 59.89$ Ω, $X_1 = -j78.04$ Ω, $X_2 = j51.46$ Ω. There was no need to use a free element – an input line segment with parameters Z_{1S} and θ_{1S1}, therefore the values of these parameters are not given. To implement dual-frequency reactive elements, line segments were used, namely: for the element jX_{1i} – a short-circuited stub with a characteristic impedance of 55.78 Ω and an electrical length of 56.84°; for the element jX_{2i} – an opened stub with parameters 87.85 Ω and 56.84°; for the element jX_i of isolation circuit – an opened stub with parameters 105.58 Ω and 53.53°. For the isolation circuit, a SMD 0402 (± 5%) 56 Ohm resistor with dimensions of 1×0.5 mm was used. To take into account the influence of the deviation of the nominal value of the selected resistor from the calculated value, as well as the influence of parasitic parameters of the Surface-Mounted Device (SMD) resistor with the selected size (series inductance 0.7 nH and parallel capacitance 0.03 pF), the reactance jX parameters of the isolation circuit were recalculated. This changed the characteristic impedance of the stub, which implements the reactance, by 3%, and its electrical length by 6.3%. The schematic-level simulations showed that these changes do not significantly affect the characteristics and width of the balun's operating bands, only slightly reducing the isolation level at a frequency of 5.2 GHz to -24 dB, which is further compensated at the electromagnetic (EM) simulation, where the resistor is modeled by a resistive film with the specified dimensions within the contact pads.

Fig. 4(a) shows the results of schematic-level simulations of this balun using the line segments physical dimensions obtained after converting the calculated electrical parameters. As can be seen, the balun has two frequency bands centered at 2.4 and 5.2 GHz. Both bandwidths at $|S_{11}| = -10$ dB are 280 MHz. Good port matching and outputs isolation are also provided.

The presence of T-junctions, bends, and open ends of transmission lines in the balun structure, which is not taken into account at the calculation stage and which degrades the balun's responses, significantly in the second passband, requires compensation for the influence of these discontinuities. Such compensation was carried out at the level of EM simulation by optimizing the parameters of line segments. A comparison of the physical dimensions of the segments obtained by the formulas with their final optimized values in percentage deviation shows the following. The width of the stripes of almost all line segments has not changed, except for segments with Z_1 and Z_{2L}, in which the deviation is +6% and −6%, respectively. The length of the strips has changed in all segments. This is explained by their direct connection with T-junctions. The reduction of it influence is precisely achieved by selecting the length of the segments. On average, such deviations did not exceed −4%, except for segments with θ_{21} and θ_{31} (−6.5% and 15%, respectively), connected to unequal T-junctions, as well as segments that implement the reactance jX_{1i} (−10%), which is explained by the influence of the grounding contact pads. The final appearance of the fabricated balun is shown in Fig. 4(b), where the areas that perform the

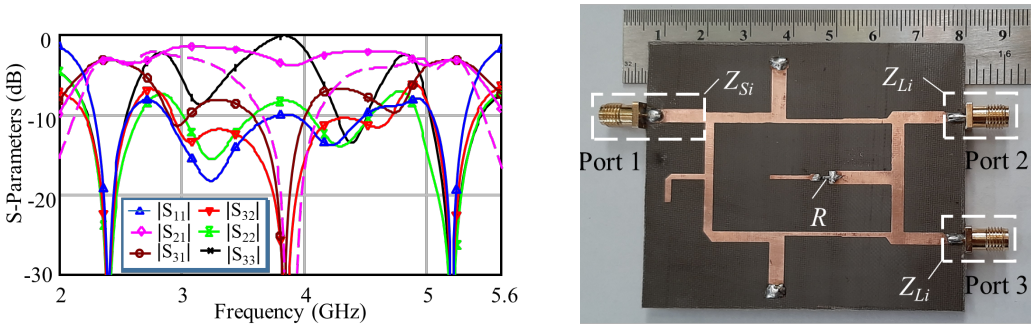

(a) (b)

Fig. 4. (a) Results of schematic-level simulations, (b) photograph of the fabricated balun

function of the given input and load impedances are highlighted. The overall size is approximately 74 × 68 mm.

The results of EM simulation and Vector Network Analyzer (VNA) measurement of S-parameters, which are delineated in Fig. 5 and Fig. 6 separately for each frequency band, are in good agreement with each other.

As can be seen from Fig. 5, after taking into account the effect of discontinuities, the balun with adjusted dimensions, when the return loss at port 1 is larger than 10 dB, provides a simulated operating bandwidth of 230/220 MHz in two bands with center frequencies 2.4/5.2 GHz. The return loss of S_{11} at these frequencies is lower than −28 dB and the insertion losses of S_{21}/S_{31} in both cases are $-3.12/-3.07$ and $-3.10/-3.26$ dB, respectively. The maximum level of outputs matching (characteristics of S_{22} and S_{33}) in the first band is achieved at the center frequency of 2.4 GHz, and in the second band – near the frequency of 5.25 GHz. The maximum value of outputs isolation S32 is below of −23 dB at both center frequencies.

Similar results can be seen from the dependencies shown in Fig. 6. As in the previous case, the fabricated balun exhibits two frequency bands with centers 2.4 and 5.2 GHz, but with slightly wider bandwidths, equal in both cases to 290 MHz (from 2.27 to 2.56 GHz in the first band and from 5.06 to 5.35 GHz in the second band at a level $|S_{11}| < -10$ dB). The measured insertion losses of $|S_{21}|/|S_{31}|$ at the two output ports are $-3.86/-3.72$ dB at 2.4 GHz and $-4.21/-4.76$ dB at 5.2 GHz. At the same time, the return loss of $|S11|$ reaches to −27 and −20 dB at these working frequencies, respectively. As at the EM simulation, the maximum matching of outputs S_{22} and S_{33} is achieved at a frequency of 2.4 GHz, and in the second band, it is shifted to a frequency of 5.3 GHz. Simultaneously, the outputs isolation $|S_{32}|$ is lower than −25 dB at both center frequencies.

Checking the designed balun for compliance with the conditions of equal amplitude of the signals at the outputs and their 180-degree phase difference gave the results obtained based on measurements, which are shown in Fig. 7 in the form of an imbalance $|S_{21}|-|S_{31}|$ of amplitude and $\angle S_{21} - \angle S_{31}$ of phase at the balun outputs in two frequency bands.

From the measurement results and Fig. 7 it follows that the mismatches in amplitude and 180°-phase difference of no more than 0.3 dB and ± 2.5° are achieved in the first above frequency band from 2.27 GHz to 2.53 GHz, and no more than 0.6 dB and ± 5° in the second band from 5.07 GHz to 5.37 GHz. At the center frequencies of the bands, the measured amplitude/phase imbalance values are 0.14 dB/−1.8° at 2.4 GHz and 0.55 dB/1.4° at 5.2 GHz.

Minor discrepancies between the EM simulation results and measurements — particularly in the second frequency band – are attributed to deviations in substrate parameters (dielectric constant and thickness) from the nominal values used in calculations, conductor losses, and PCB manufacturing inaccuracies.

Table 1 compares the performance of the proposed balun with those of the best recently developed dual-band baluns. As shown, the proposed balun demonstrates high-level performances that are not inferior to the results of the listed designs. Moreover, this is achieved simultaneously with providing a dual-band transformation of complex impedances, the implementation of which leads to a significant complication of the balun circuit compared to the case of real impedances transformation.

Conclusions

This paper has presented a dual-band balun based on branch-line structure with shunt stubs. One of the key features of the proposed balun is its ability to provide impedance transformation integrated with balun operation for a wide range of complex source and load impedances with frequency-dependent values. To enable this capability, additional elements with arbitrarily selectable electrical parameters have been introduced into the balun structure. Furthermore, this approach allows for the implementation of a device with any desired frequency ratio. Complete design formulas for this balun were derived using the even-odd mode method. To verify the design concept, an experimental prototype was fabricated; the measurement results show excellent agreement with

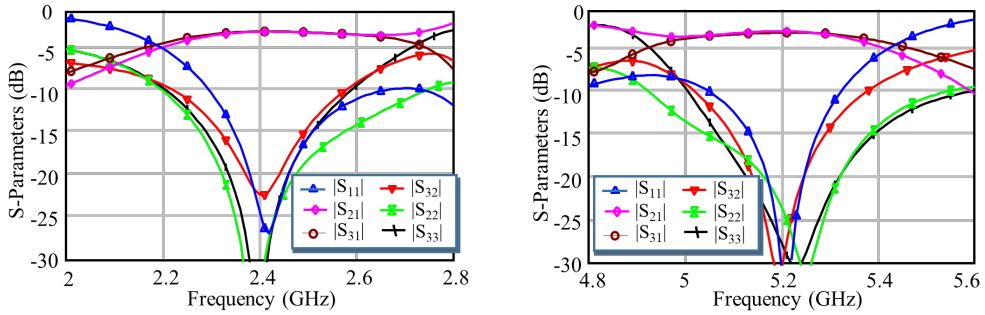

Fig. 5. Simulated scattering parameters at: (a) 2.4- and (b) 5.2-GHz bands

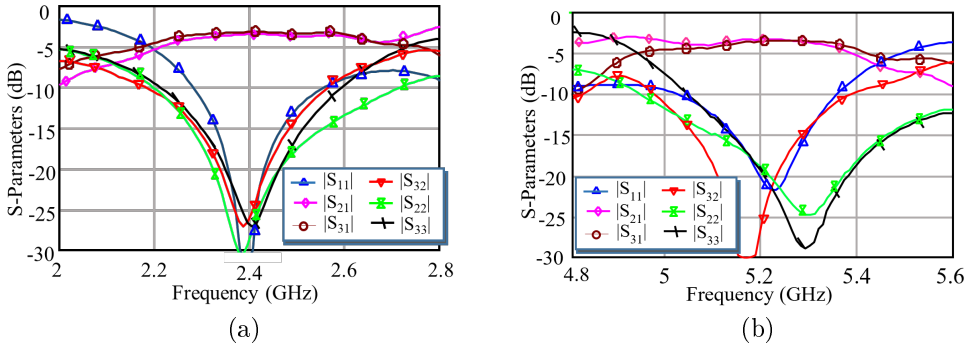

Fig. 6. Measured scattering parameters at: (a) 2.4- and (b) 5.2-GHz bands

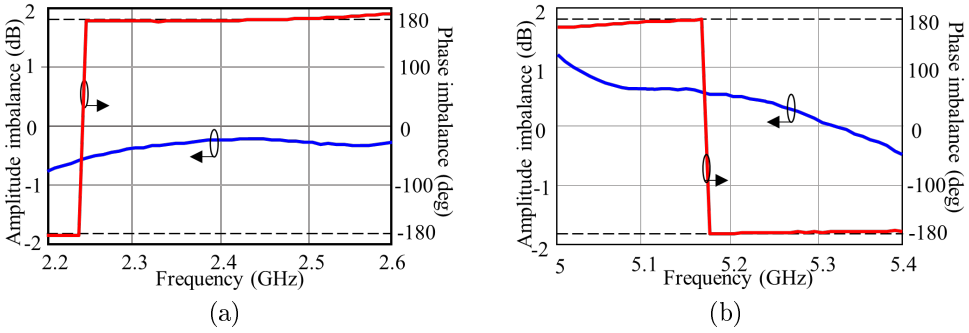

Fig. 7. Imbalance of amplitude and phase at the balun outputs at: (a) 2.4- and (b) 5.2-GHz bands

Table 1 Comparison of proposed balun performance with the existing state-of-the-art designs

Param.\Ref.	[4]	[5]	[8]	**Present**
f_1/f_2 (GHz)	2.39/5.1	1/2	1.42/2.82	2.4/5.2
$\|S_{21}\|$ (dB)	−3.46/−4.17	−3.5/−3.8	−3.48/−3.57	−3.86/−4.21
$\|S_{31}\|$ (dB)	−3.45/−4.17	−3.3/−3.8	−3.28/−3.77	−3.72/−4.76
$\|S_{11}\|$ (dB)	−36/−25	−26/−28	−25/−19	−27.2/−20.1
FBWs (%), RL (<-10 dB)	15/4.9	13/6.5	12/5.7	12.1/5.6
$\angle S_{21}-\angle S_{31}$ (°)	179/181	181/180	179.1/180.2	178.2/178.6
Isolation (dB)	−28/−26	−26/−26	39/32	−27/−27
Function of impedance transformation	Real to real	Real to real	Complex to real	Complex to complex

simulation outcomes, thereby confirming the feasibility of the proposed methodology. The results demonstrate that the dual-band balun provides a high level of port matching and isolation between the balanced outputs, making it highly suitable for applications in microwave communication circuits.

References

[1] Gorur, A. K. (2020). A Dual-Band Balun BPF Using Codirectional Split Ring Resonators. *IEEE Microwave and Wireless Components Letters*, Vol. 30, Iss. 10, pp. 949–952. DOI:10.1109/LMWC.2020.3016622.

[2] Ge, J., Jiang, W., and Wang, G. (2021). A Dual-Band Balun BPF Using Double-Sided Parallel-Strip Line. *2021 IEEE MTT-S International Microwave Symposium (IMS), 07-25 June 2021*, Atlanta, GA, USA, pp.251-253. DOI: 10.1109/IMS19712.2021.9574948.

[3] Xiao, J.-K., Wu, R.-T., and Li, X.-F. (2024). Self-Packaged Wideband Filtering Baluns Based on Suspended Coplanar Waveguide-Microstrip Hybrid. *IEEE Transactions on Components, Packaging and Manufacturing Technology*, Vol. 14, Iss. 3, pp. 489-500. DOI: 10.1109/TCPMT.2024.3366612.

[4] Li, E. S., Lin, C.-T., Jin, H., and Chin, K.-S. (2019). A systematic design method for a dual-band balun with impedance transformation and high isolation. *IEEE Access*, Vol. 7, pp. 143805-143813. DOI: 10.1109/ACCESS.2019.2945049.

[5] Gupta, R., Hashmi, M. S., and Chaudhary, M. A. (2020). Flexible design scheme for a simple dual-band ultra-high impedance transformer and its application in a balun. *IEEE Access*, Vol. 8, pp. 125745-125754. DOI: 10.1109/ACCESS.2020.3008046.

[6] Gupta, R., Kairatova, S., Hashmi, M., and Nauryzbayev, G. (2021). A dual-band balun architecture with unequal port-terminations. *50th European Microwave Conference (EuMC) (IEEE, 2021), 12–14 Jan. 2021*, Utrecht, Netherlands, pp. 848–851. DOI: 10.23919/EuMC48046.2021.9337973.

[7] Maktoomi, M. H., Ren, H., Marbell, M. N., Klein, V., Wilson, R., and Arigong, B. (2020). A wideband isolated real-to-complex impedance transforming uniplanar microstrip line balun for push–pull power amplifier. *IEEE Trans. Microw. Theory Tech.*, Vol. 68, No. 11, pp. 4560-4569. DOI: 10.1109/TMTT.2020.3019003.

[8] Oborzhytskyy, V. I., Storozh, V. H., and Fabirovskyy, S. Ye. (2023). Dual-band Microstrip Balun with Different Complex Load Impedances in Frequency Bands. *Radioelectronics and Communications Systems*, Vol. 66, No. 1, pp. 1–14. DOI: 10.3103/S0735272723030044.

[9] Oborzhytskyy, V., Fabirovskyy, S., and Sidelnyk, I. (2024). Design method of a dual-band balun, loaded with frequency-dependent complex impedances. *17th International Conference on Advanced Trends in Radioelectronics, Telecommunications and Computer Engineering (TCSET)*, Lviv-Slavsko, Ukraine, 09-12 Octob., pp. 1-4. DOI: 10.1109/TCSET64720.2024.10755514.

[10] Li, E. S., Lin, C.-T., Jin, H., and Chin, K.-S. (2019). A Broadband Balun With Complex Impedance Transformation and High Isolation. *IEEE Access*, Vol. 7, pp. 112295-112303. DOI: 10.1109/ACCESS.2019.2934506.

[11] Tang, D., Luo, X. (2021). Compact Filtering Balun With Wide Stopband and Low Radiation Loss Using Hybrid Microstrip and Substrate-Integrated Defected Ground Structure. *IEEE Microwave and Wireless Components Letters*, Vol. 31, No. 6, pp. 549-552. DOI:10.1109/lmwc.2021.3065416.

[12] Deb, P. K., Moyra, T., and Bhattacharyya, B. K. (2021). Miniaturized and enhanced bandwidth Marchand balun using CSRR. *IET Microw. Antennas Propag.*, Vol. 15, Iss. 7, pp. 788–796. DOI: 10.1049/mia2.12086.

[13] Steele, J., Psychogiou, D. (2024). Wideband Broadside-Coupled Line Baluns Enabled by Multimaterial Additive Manufacturing. *IEEE Trans. Microw. Theory Tech.*, Vol. 72, No. 10, 2024, pp. 5904-5916. DOI: 10.1109/TMTT.2024.3392434.

[14] Ke, Y.-H., Yang, L.-L., and Chen, J.-X. (2021). Design of Switchable Dual-Balun Feeding Structure for Pattern-Reconfigurable Endfire Antenna. *IEEE Antennas and Wireless Propagation Letters*, Vol. 20, Iss. 7, pp. 1463-1467. DOI:10.1109/LAWP.2021.3087479.

[15] Yu, Y.-Q., Jiang, W., Qin, L., Shao, H.-Y., and Gong, S.-X. (2020). Design of a Planar Transmission Line Balun Based on Novel Phase Inverter. *IEEE Access*, Vol. 8, pp. 18915 – 18924. DOI:10.1109/ACCESS.2020.2968341.

[16] Zhang, W., Wu, Y., Liu, Y., Yu, C., and Chen, W. (2015). Compact coupled-line balun with complex impedances transformation and high isolation. *IET Microwaves, Antennas Propag.*, Vol. 9, Iss. 14, pp. 1587-1594. DOI: 10.1049/iet-map.2014.0775.

[17] Zhang, W., Wu, Y., Wang, W., and Shen, X. (2017). Planar compact dual-band coupled-line balun with high isolation. *China Commun.*, Vol. 14, No. 2, pp. 40-48. DOI: 10.1109/CC.2017.7868173.

[18] Gupta, R., Hashmi, M. (2018). High impedance transforming simplified Balun architecture in microstrip technology. *Microw. Optical Technol. Lett.*, Vol. 60, Iss. 12, pp. 3019-3023. DOI: 10.1002/mop.31450.

[19] Wu, Y., Yao, L., Zhang, W., Wang, W., and Liu, Y. (2016). A planar dual-band coupled-line balun with impedance transformation and high isolation. *IEEE Access*, Vol. 4, pp. 9689-9701. DOI: 10.1109/ACCESS.2016.2640187.

[20] Oborzhytskyy, V., Protasevych, V., Storozh, V., and Khiblin, O. (2024). Microstrip dual-band transformer of complex load impedances into complex input impedances with different values in frequency bands. *17th International Conference on Advanced Trends in Radioelectronics, Telecommunications and Computer Engineering (TCSET)*, Lviv-Slavsko, Ukraine, 09-12 Octob., pp. 574-577. DOI: 10.1109/TCSET64720.2024.10755665.

[21] Prudyus, I., Oborzhytskyy, V. (2017). Dual-band devices based on coupled striplines for different power distribution in the frequency bands. *Radioelectronics and Communications Systems*, Vol. 60, No. 12, pp. 545–554. DOI: 10.3103/S0735272717120044.

Мікросмужковий двосмуговий балун шлейфного типу з довільними в смугах комплексними частотно-залежними імпедансами входу та навантаження

Оборжицький В. І., Фабіровський С. Є., Сторож В. Г., Матієшин Ю. М., Банщикова Т. Є.

У статті запропоновано структуру планарної мікросмужкової схеми для проєктування компактного двосмугового балуна, два вихідні сигнали якого мають однакові амплітуди та протилежні фази у двох робочих діапазонах частот. Водночас така схема забезпечує трансформацію комплексних імпедансів навантаження, різних у цих діапазонах, у комплексні вхідні імпеданси джерела, які також відрізняються у цих діапазонах. Запропонована схема балуна ґрунтується на симетричній чотирипортовій структурі шлейфного типу з одним відкритим портом, утвореній відрізками одиночної лінії передачі з трьома реактивними елементами та схемою розв'язки. Для реалізації цих реактивних елементів зі значеннями, різними у частотних діапазонах, використовуються відгалуження з відрізків ліній передачі. Завдяки застосуванню до симетричної чотирипортової структури аналізу в режимі парної і непарної мод було отримано вирази для розрахунку електричних параметрів елементів схеми двосмугового балуна. Для усунення обмежень на значення допустимих для трансформації комплексних імпедансів (як навантажень, так і вхідного) у схему також введено додаткові відрізки ліній, параметри яких задаються довільно. Вибір значень цих параметрів дозволяє в результаті розрахунків отримати значення електричних параметрів відрізків ліній схеми, які придатні для їх технічної реалізації. З метою перевірки запропонованої схеми та методу розрахунку було реалізовано і досліджено прототип двосмугового балуна, що працює на частотах 2,4 та 5,2 ГГц. Для виготовлення балуна на основі мікросмужкових ліній передачі використано діелектричну підкладку з діелектричною проникністю 2,6 і товщиною 1,45 мм. Вимірювання показали, що розбалансування амплітуд і відхилення різниці фаз від 180° є меншими, ніж 0,6 дБ і 5° відповідно, смуга пропускання двосмугового балуна становить 290 МГц в обох діапазонах. Як результати моделювання, так і результати вимірювань добре узгоджуються, що доводить правильність запропонованої концепції проєктування.

Ключові слова: балун; двосмуговий режим роботи; метод парного-непарного збудження; частотно-залежні вхідні та навантажувальні імпеданси; перетворення комплексного імпедансу